SIMULATION OF POLYMER FLOW DURING FUSED FILAMENT FABRICATION

Parties prenantes

Institut Mines-Télécom

IMT Mines Alès
École Mines-Télécom

Auteurs

Arnaud Regazzi.
Jean-Christophe Quantin.
Anirudha Jain

Partenaires

cnrs

INTRODUCTION

Unlike molding processes, **additive manufacturing** processes have few or no dedicated **digital simulation tools**. However, these tools are essential to predict the behavior of materials during their implementation and thus avoid tedious trial and error tests. In the case of **FFF**, several causes can lead to manufacturing failure. Among them, the risk of **filament buckling** or **grinding** can be important. Yet the occurrence of these phenomena is mostly dependent on the reaction force that the filament undergoes. Hence, the purpose of this study is to simulate the **polymer flow** in a FFF nozzle in order to predict the pressure drop and therefore the **reaction load** exerted on the filament at the hot end inlet.

MATERIALS AND METHODS

- **System**: the hot end of an A4v3 machine (cf. Figure 1) from the company 3ntr (Oleggio, Italy)
- **Software**: COMSOL Multiphysics®
- **Geometry**: geometry and boundary conditions provide a revolution symmetry, allowing to consider a 2D axi-symmetric model (cf. Figure 2).
- **Material**: PLA Ingeo™ 7000D from NatureWorks®

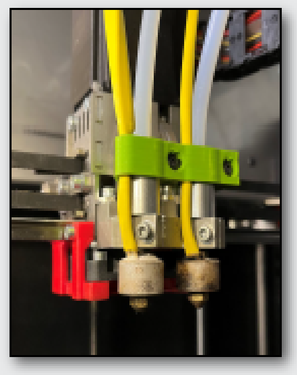

Figure 1. Picture of the print head with its two hot ends inside the printer

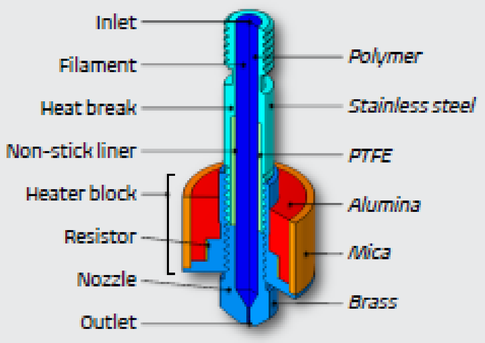

Figure 2. Schematic of the hot end considered for the simulation with its components and materials

POLYMER FLOW

Polymer density was temperature dependent but not pressure dependent, resulting in a weakly compressible flow.
In all the polymer domains, the **Navier-Stokes equations** for **laminar flow** were solved:

$$\frac{\delta \rho}{\delta t} + \nabla \cdot (\rho \mathbf{u}) = 0$$
$$\rho \frac{\delta \mathbf{u}}{\delta t} + \rho (\mathbf{u} \cdot \nabla)\mathbf{u} = \nabla \cdot [-p\mathbf{I} + \mathbf{K}]$$
$$\mathbf{K} = \mu\left(\nabla \mathbf{u} + (\nabla \mathbf{u})^T\right) - \frac{2}{3}\mu(\nabla \cdot \mathbf{u})\mathbf{I}$$

p is the pressure (Pa)
$\mathbf{u}$ is the velocity field (m.s^{-1})
$\mathbf{K}$ is the deviatoric stress tensor
$\mathbf{I}$ is the identity tensor (-)
ρ is the density (kg.m^{-3})
μ is the dynamic viscosity (Pa.s)

Dynamic viscosity was shear-rate and temperature dependent, resulting in the choice of a **Cross-WLF** model:

$$\mu(\dot{\gamma}, T) = \frac{\mu_0(T)}{1 + \left(\mu_0(T)\frac{\dot{\gamma}}{\tau^*}\right)^{1-n}}$$
$$\mu_0(T) = D_1 \exp\left(-\frac{A_1(T - T^*)}{A_2 + (T - T^*)}\right)$$

$\dot{\gamma}$ is the shear rate (s^{-1})
T is the temperature (K)
μ_0 is the zero-shear viscosity (Pa.s)
n is the power law index in high shear rate regime: 0,25
τ^* is the critical stress level at the transition to shear thinning: 100.86 kPa
T^* is the reference temperature: 373.15 K
A_1, A_2, D_1 are experimentally fitted coefficients: 20.19, 51.6 K, and 3.317 GPa.s

Boundary conditions:
- Slip condition ($\mathbf{u} \cdot \mathbf{n} = 0$) between polymer and PTFE or stainless steel
- Non-slip condition ($\mathbf{u} = 0$) between polymer and brass
- Velocity field at the inlet controlled by the solving sequence (cf. solver)
- Pressure at the outlet set to zero with no backflow allowed

CONDUCTIVE HEAT TRANSFER

Polymer thermal conductivity and **heat capacity** were temperature dependent, unlike the other materials.
In all the hot end domains, the **heat equation** and **Fourier's law** were solved:

$$\rho C_p \frac{\delta T}{\delta t} + \rho C_p \mathbf{u} \cdot \nabla T + \nabla \cdot \mathbf{q} = Q$$
$$\mathbf{q} = -k\nabla T$$

T is the temperature (K)
$\mathbf{u}$ is the velocity field (m.s^{-1})
$\mathbf{q}$ is the heat flux density (W.m^{-2})
Q is the volumetric heat source (W.m^{-3})
k is the thermal conductivity (W.m^{-1}.K^{-1})
ρ is the density (kg.m^{-3})
C_p is the heat capacity (J.kg^{-1}.K^{-1})

Boundary conditions:
- Convective heat flux ($\mathbf{n} \cdot \mathbf{q} = h(T - T_{amb})$) between external boundaries and air at T_{amb} = 25 °C.
- Conductance between the heat break and the heat sink (not represented)
- Thin resistive layers between brass, stainless steel and alumina.

Heat sources:
- Joule effect in the resistor: current intensity was controlled by a PID controller for which temperature was provided by a probe embedded in the alumina
- Viscous dissipation within the polymer due to shear stress ($Q_{vd} = \mathbf{K} \cdot \nabla \mathbf{u}$)

SOLVER

The **time dependent** simulations were carried out in **2 steps** which used implicit, direct and fully coupled solvers:
1. The hot end was **heated up** from the uniform, ambient initial temperature. When the temperature at the tip of the PT100 probe approached the **set temperature** ($T_{set} - T(t) < 1[K]$), a **stop condition** was activated for the solver, which triggered the second step
2. The PID controller kept the **temperature constant** at the tip of the PT100 probe and the **filament was moved** progressively from still to 1 mm.s^{-1} over 2 s. The solver was stopped after 60 s.

RESULTS

- **Temperature gradients**: important, as expected, in the axial direction, but also in the radial direction (cf. Figure 3).
- **Pressure gradients**: negligible in most of the hot end channel; the pressure drop responsible for the compression reaction force exerted on the incoming filament occurs mostly within the capillary (cf. Figure 4).
- **Polymer within the capillary**: at T_{set} = 200 °C and at mid-length of the capillary, the polymer velocity is uniform over a radius of 0.1 mm (cf. Figure 5). Shear rate reaches 2800 s^{-1} on the capillary wall.
- **Compression reaction force**: decreases drastically with T_{set} (cf. Figure 6). Regardless of T_{set}, a peak is observed when the filament is set in motion, after which the force decreases more or less depending on T_{set}. Then the force increases again under the effect of the incoming colder polymer, before reaching a plateau corresponding to steady state.

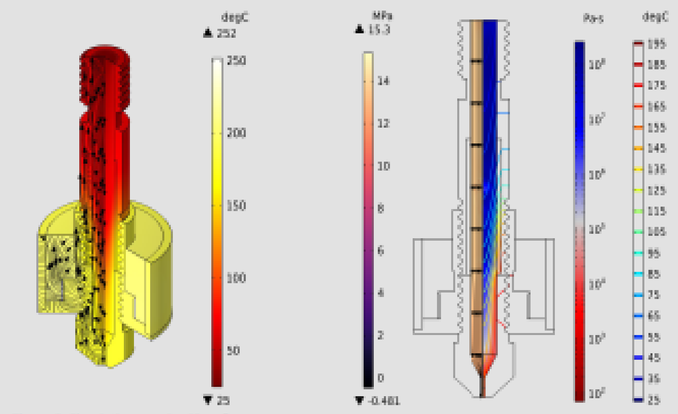

Figure 3. Simulation results 60 s after reaching T_{set} = 200 °C
Heat flux density streamlines overlaying the temperature field

Figure 4. Simulation results 60 s after reaching T_{set} = 200 °C
Left: velocity streamlines overlaying the pressure field
Right: isotherms overlaying viscosity distribution

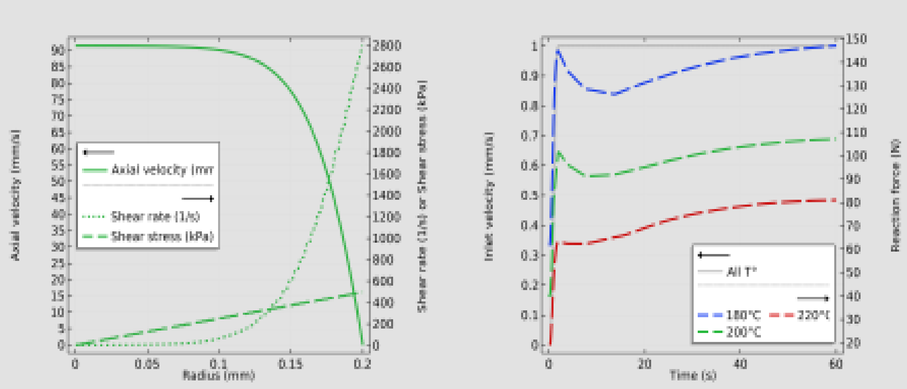

Figure 5. Simulation results 60 s after reaching T_{set} = 200 °C
Axial velocity (left), shear rate and stress (right) at mid-length of the capillary channel along its radius

Figure 6. Time dependent simulation results after reaching T_{set}
Filament velocity at the heat break inlet (left) and resulting reaction force as a function of T_{set} (right)

CONCLUSION

The influence of the **nozzle temperature**, **filament velocity** and **shape of the nozzle** on processing conditions can be assessed with this simulation. Though **results are consistent** with the expected orders of magnitude, **measurements** need to be carried out to adjust the model or its inputs, and eventually prove its reliability.

Contact : Contact Arnaud Regazzi : arnaud.regazzi@mines-ales.fr

Mars 2023 - Colloque de l'Institut Mines Télécom Mines Saint-Etienne (Campus Région du numérique, Charbonnières-les-Bains)